Control Strategy of Single-Phase Active Front-End Cascaded H-Bridge Under Cell Fault Condition

Yoon-Ro Lee, *Student Member, IEEE*, Jeong-Mock Yoo, *Member, IEEE*, Hyun-Sam Jung, *Student Member, IEEE*, and Seung-Ki Sul, *Fellow, IEEE*

***Abstract*—Cascaded H-bridge (CHB) inverter is the most widely used topology for a medium-voltage drive system due to the high degree of modularity, easier implementation of medium output voltage, and the ability to continuous operation under the cell fault condition. Because each power cell of CHB should have isolated dc source, multiwinding input transformer and three-phase active front end (AFE) are generally used for regenerative applications. The whole system can be simplified by replacing the three-phase AFE with single-phase AFE. However, if the control strategy of normal operation is adopted under the cell fault condition, input power imbalance among three phases inevitably occurs. In that situation, not only faulty cells, but also some unscathed cells should be excluded with giving up the maximum capability of the system, not to deteriorate grid current. This paper proposes a control scheme against the cell fault condition of the single-phase AFE CHB. By applying the proposed control scheme to the system, dc-link voltage of each cell and grid current are well regulated without imbalance even under the cell fault conditions. Finally, it can minimize the number of undamaged cells which should be turned OFF and maximize the capability of the system under the cell fault condition. Simulation and experimental results are provided to verify the effectiveness of the proposed scheme.**

***Index Terms*—Active and reactive coordinate transformation (ARCX), current control, dc-link voltage control, fault operation pair, negative sequence current control, normal operation pair, power factor, three-phase balanced grid current.**

I. Introduction

ONE of the most widely used multilevel inverter topologies for medium-voltage (MV) drive is the cascaded H-bridge (CHB) inverter [1]. CHB inverter has several advantages such as high degree of modularity, easier implementation of medium output voltage with relatively low voltage components, low current harmonic distortion, and higher availability [2]–[4]. In addition, one of the most notable features of CHB topology is that it could be continuously operated under the cell fault condition. The cell fault, conventionally considered in CHB systems, can be categorized as dc-link overvoltage (OV) or undervoltage (UV) fault, junction over-temperature (OT) fault, arm-short or

Manuscript received March 6, 2018; revised May 20, 2018; accepted July 9, 2018. Date of publication July 19, 2018; date of current version March 29, 2019. This paper was financially supported by Seoul National University Electric Power Research Institute. Recommended for publication by Associate Editor M. T. Bina. *(Corresponding author: Yoon-Ro Lee.)*

The authors are with Seoul National University, Seoul 151-744, South Korea (e-mail:

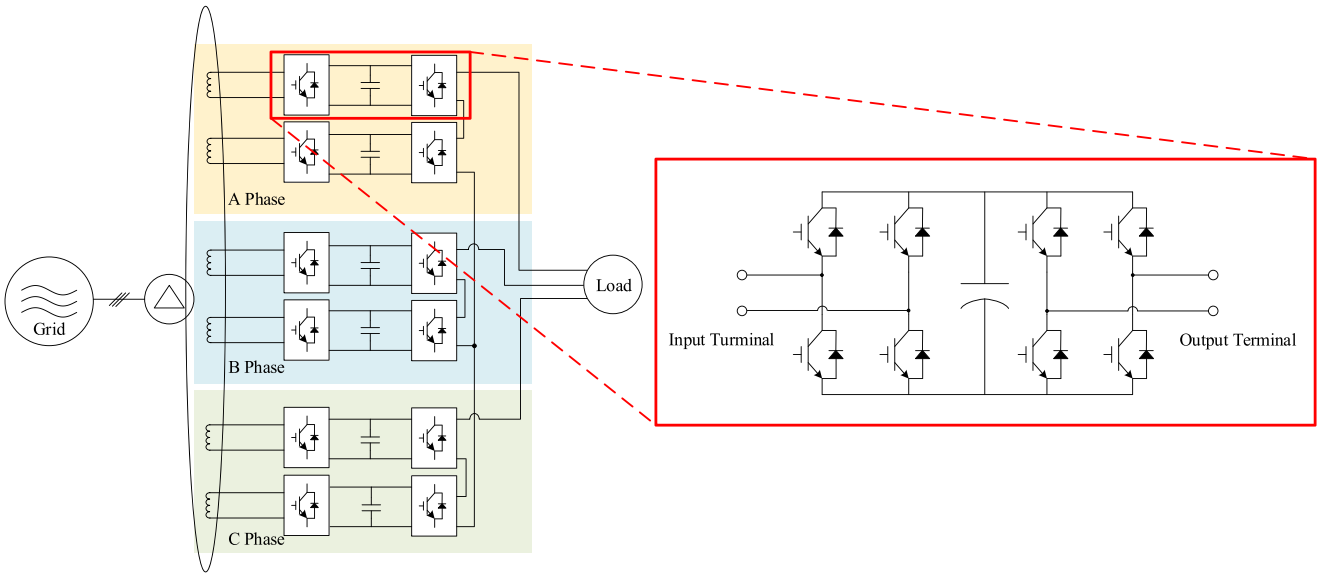

Fig. 1. Circuit of single-phase AFE CHB and its power cell structure.

stages and performs the input power control and dc-link voltage control in individual stages independently. In this paper, one stage is denoted as a normal operation pair, and the three-phase input current of the pair is controlled as three-phase balanced current by the method. However, if the cell fault occurs and some faulty cells are disconnected from the single-phase AFE CHB, there could be some healthy power cells which cannot mate the normal operation pair with any other power cells. Then, the control method for the normal operation pair [10] cannot be adopted to the unfortunate power cells for their input power and dc-link voltage control. Under this situation, each unfortunate cell could drive its input structure as an independent single-phase H-bridge converter with any conventional single phase input power control schemes such as [11]. Then, all of the healthy cells under the cell fault condition could be used. Therefore, the maximum utility of the system could be achieved by not detaching any healthy cells and the magnitude of the output voltage can be extended as much as possible. However, unlike the conventional three-phase DFE CHB or three-phase AFE CHB, the independent input power control of a single power cell would cause the severe deterioration of the grid current with huge amount of negative sequence current. Accordingly, this method cannot be an option.

The only available suggestion for the single-phase AFE CHB under the cell fault would be maintaining the number of cells per each phase as the same, by detaching not only the faulty cells but also some healthy cells from the system. As the results, the control strategy for a normal operation pair [10] can be adopted for the system even under the cell fault condition with three-phase balanced grid current. However, in the suggestion, the system cannot synthesize maximum output voltage and cell usage is significantly degraded. It makes the capacity of the single-phase AFE CHB be reduced seriously.

Therefore, a novel reconfiguration scheme with new control methods of input power and dc-link voltage for a single-phase AFE CHB system is proposed in this paper to guarantee its maximum output voltage range and power capacity under cell fault conditions. Besides, even under the cell fault condition, with the proposed method, dc-link voltage of each cell is successfully regulated as its reference value and all three-phase grid currents are also well balanced.

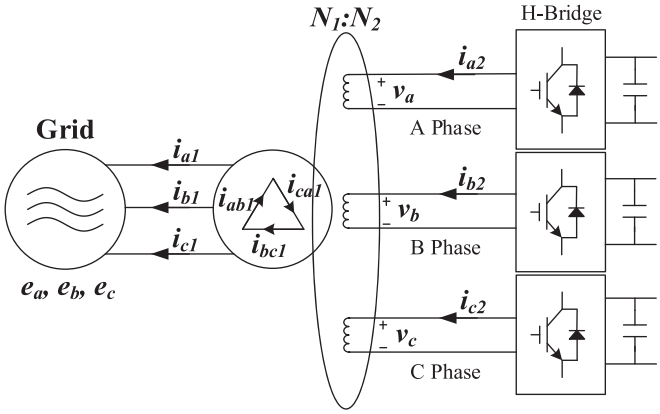

Fig. 2. Input transformer and single-stage input structure of single phase AFE CHB.

II. Analysis of Cell Fault Condition and Reconfiguration Strategy

To simplify analysis about the relation between the grid currents, i_{a1}, i_{b1}, and i_{c1}, and the converter currents, i_{a2}, i_{b2}, and i_{c2}, the single-phase AFE CHB is configured as single stage as shown in Fig. 2. Also, it is assumed that transformer is ideal, which has no excitation current, no leakage fluxes, no losses, and balanced three-phase windings. The primary delta winding currents, i_{ab1}, i_{bc1}, and i_{ca1}, are coupled with the converter currents, i_{a2}, i_{b2}, and i_{c2}, respectively. Grid phase voltages are

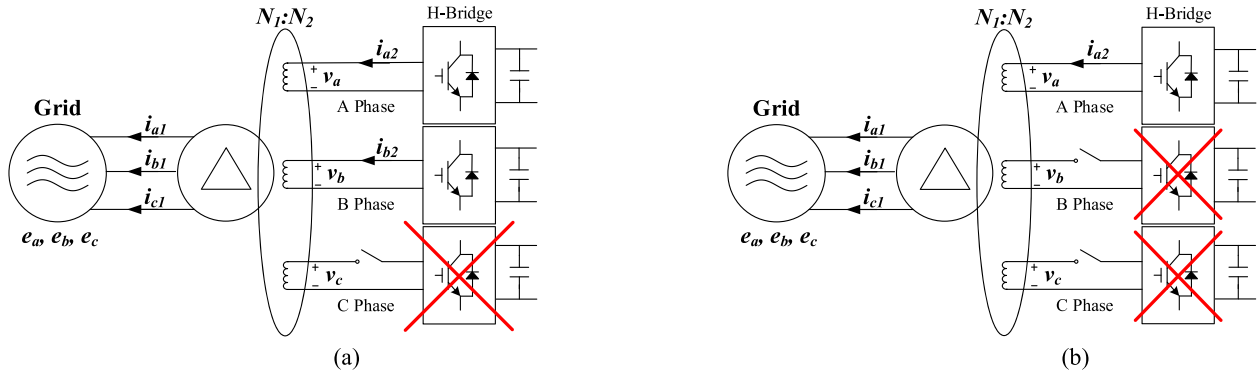

Fig. 3. Two kinds of cell fault conditions in a single-stage system. (a) One cell fault condition. (b) Two cells fault condition.

represented as e_a, e_b, and e_c. The primary side of the input transformer is connected in delta winding to handle third harmonic current from the excitation current of the transformer. If N_1 and N_2 are the numbers of turns in the primary winding and the secondary winding, respectively, the relation between grid currents and converter currents can be described as follows under the assumption of an ideal transformer

$$\begin{aligned} i_{a1} &= i_{ab1} - i_{ca1} = \frac{N_2}{N_1} i_{a2} - \frac{N_2}{N_1} i_{c2} \\ i_{b1} &= i_{bc1} - i_{ab1} = \frac{N_2}{N_1} i_{b2} - \frac{N_2}{N_1} i_{a2} \\ i_{c1} &= i_{ca1} - i_{bc1} = \frac{N_2}{N_1} i_{c2} - \frac{N_2}{N_1} i_{b2}. \end{aligned} \tag{1}$$

The circulating current of delta winding, i_{circ}, could be represented with the converter currents as

$$i_{\text{circ}} = \frac{i_{ab1} + i_{bc1} + i_{ca1}}{3} = \frac{N_2}{3N_1} \cdot (i_{a2} + i_{b2} + i_{c2}). \tag{2}$$

If the converter current is controlled as three-phase balanced current, the circulating current would be zero.

On the other hand, analysis about the cell fault conditions which can occur in a single-stage system would be carried out with (1). Fault conditions can be classified into two types according to the number of faulty cells in a stage, as shown in Fig. 3. Fig. 3(a) shows one cell fault condition. In this figure, because a cell of *C* phase is a faulty cell, the input terminal of the faulty cell is disconnected from the grid and input current of the faulty cell, i_{c2}, becomes zero. Therefore, in this case, (1) can be rewritten as

$$\begin{aligned} i_{a1} &= \frac{N_2}{N_1} i_{a2} \\ i_{b1} &= \frac{N_2}{N_1} i_{b2} - \frac{N_2}{N_1} i_{a2} \\ i_{c1} &= -\frac{N_2}{N_1} i_{b2}. \end{aligned} \tag{3}$$

In that situation, the remaining converter currents, i_{a2} and i_{b2}, are proposed to be regulated as

$$\begin{aligned} i_{a2} &= I_m \cos(\omega t + \phi) \\ i_{b2} &= I_m \cos(\omega t - 60^\circ + \phi). \end{aligned} \tag{4}$$

Then, the grid currents, i_{a1}, i_{b1}, and i_{c1}, can be represented as (5), by substituting (4) into (3)

$$\begin{aligned} i_{a1} &= \frac{N_2}{N_1} I_m \cos(\omega t + \phi) \\ i_{b1} &= \frac{N_2}{N_1} I_m (\cos(\omega t - 60^\circ + \phi) - \cos(\omega t + \phi)) \\ &= \frac{N_2}{N_1} I_m \cos(\omega t - 120^\circ + \phi). \\ i_{c1} &= -\frac{N_2}{N_1} I_m \cos(\omega t - 60^\circ + \phi) \\ &= \frac{N_2}{N_1} I_m \cos(\omega t + 120^\circ + \phi). \end{aligned} \tag{5}$$

Based on this analysis from (3) to (5), the grid current could be regulated as three-phase balanced current in one cell fault condition, if converter currents of the two remaining cells are regulated with the same magnitudes and 60° phase delay like (4).

Fig. 3(b) shows the two cells fault condition. Because the cells of *B* phase and *C* phase are faulty cells in this figure, i_{b2} and i_{c2} become null. Therefore, (1) would be rewritten as follows:

$$\begin{aligned} i_{a1} &= \frac{N_2}{N_1} i_{a2} \\ i_{b1} &= -\frac{N_2}{N_1} i_{a2} \\ i_{c1} &= 0. \end{aligned} \tag{6}$$

In this case, it is impossible to make the grid current of three phase be balanced by the only remaining secondary-side current, i_{a2}. Thus, the unscathed A cell should be disconnected, not to produce any negative sequence current on the grid side.

Consequently, in this paper, the control strategy of single-phase AFE CHB under cell fault condition is proposed in the one

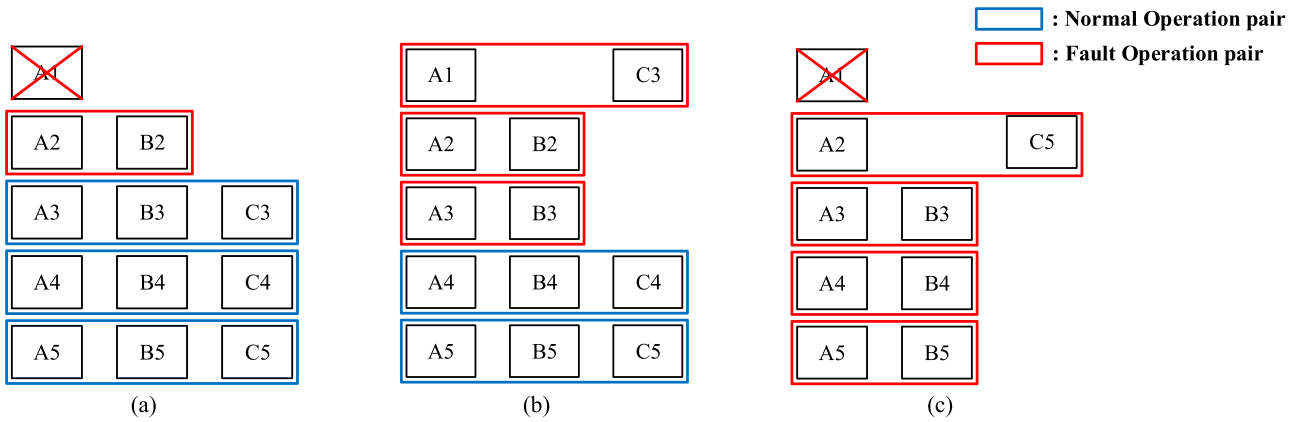

Fig. 4. Cells reconfiguration examples of (a) 5-4-3, (b) 5-4-3 (reconfigured), and (c) 5-3-1 (reconfigured) fault condition.

cell fault condition, and the two healthy cells in the condition are defined as a fault operation pair. Also, it is proposed to regulate the converter currents of the fault operation pair with the same magnitudes and 60° phase delay. However, the fault operation pair would induce the circulating current by substituting (4) into (2), expressed as

$$i_{\text{circ}} = \frac{N_2}{3N_1} \cdot (i_{a2} + i_{b2}) = \frac{N_2}{\sqrt{3}N_1} I_m \angle \phi - 30^\circ. \quad (7)$$

If the number of fault operation pairs in the single-phase AFE CHB is $\boldsymbol{N}$, the circulating current would be represented as (8) by using the superposition law, and the magnitude could be described as follows:

$$i_{\text{circ}} = \frac{N_2}{\sqrt{3}N_1} \sum_{n=1}^{N} I_{mn} \angle \phi_n - 30^\circ. \quad (8)$$

$$|i_{\text{circ}}| = \frac{N_2}{\sqrt{3}N_1} \left| \sum_{n=1}^{N} I_{mn} \angle \phi_n - 30^\circ \right|. \quad (9)$$

On the other hand, as aforementioned, in the two cells fault conditions in a stage, it is unavoidable to shut down the healthy cells. To minimize these cases, it is necessary to reconfigure the remaining healthy cells into the new normal operation pairs and fault operation pairs. As an example, in the case of CHB with five stages, if one faulty cell is in *B* phase and two faulty cells are in *C* phase as shown in Fig. 4(a), then it can be denoted as 5-4-3 fault condition, where "5-4-3" denotes number of remaining healthy cells in corresponding phase.

Before the reconfiguration of healthy cells as Fig. 4(a), normal operation pairs (A3, B3, C3), (A4, B4, C4), (A5, B5, C5), and a fault operation pair (A2, B2) are controlling their own input power and dc-link voltages, while the grid current maintains three phase balanced by using the proposed current equation (4). However, there is no reserved cell to make any pair with A1 cell, so it was expected to be shut down.

However, after the reconfiguration as shown in Fig. 4(b), C3 cell can be migrated from a normal operation pair (A3, B3, C3) to the first stage, where only A1 cell is available. The migration makes a new fault operation pair with A1 cell, and the remaining A3 and B3 cells would be recombined as a fault operation pair intentionally. Because there is no electrical connection among the input structures of power cells, but just magnetic connections through the input transformer, each power cell can be easily reconfigured from an original pair to another operation pair by manipulating its input voltage command, which is synthesized by the input H-bridge of the power cell. Finally, all unscathed cells can be used and it can maximize power capacity of the CHB converter under 5-4-3 cell fault condition.

Fig. 4(c) shows 5-3-1 fault condition. In this figure, even if power capacity is maximized by the reconfiguration, A1 cannot make any operation pair. Therefore, in this case, the healthy cell, A1, should be turned OFF inevitably.

On the other hand, the cell fault rate of a single-phase AFE CHB with five stages, which consists of 120 IGBTs and 15 dc-link capacitors, can be calculated as 140.93 [failure/10^6 h], [12]. It means that the possibility of the fault is 1.22 per a year. CHB topologies are often employed in power plant, fan and pump for manufacture factories. Therefore, stall of the system may cause stall of whole factory or plant. In order to prevent the cost penalty, it is necessary to figure out the strategy against such fault. And the proposed reconfiguration method would be helpful to increase the availability of the system under such a cell fault.

III. Implementation of Fault Operation

In single-phase AFE CHB systems, the three cells in a normal operation pair have the same power consumption. But in a fault operation pair, power consumptions of the two cells are generally different. This phenomenon would be explained in Section IV. Therefore, without proper dc-link voltage control, difference of the two dc-link voltages in a fault operation pair would become larger. It would make the CHB converter be stalled by OV or UV faults. To act against to this dc-link voltage unbalance, a dc-link voltage control method with input current control should be devised in fault operation pair.

A. Definition of Active Current and Reactive Current

In case of balanced grid voltage, phase angles of the grid phase voltages, e_a, e_b, and e_c can be denoted as 0°, –120°, and

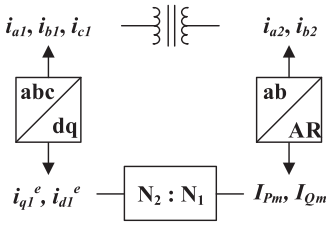

Fig. 5. Relation between d, q and ARCX.

120°, respectively. In addition, balanced three-phase current in the grid can be guaranteed by regulating converter current as (4). i_{a2} and i_{b2} described in (4) can be divided into two quadrature components as

$$\begin{aligned} i_{a2} &= I_{Pm}\cos(\omega t) + I_{Qm}\cos(\omega t - 90^\circ) = i_{Aa2} + i_{Ra2} \\ i_{b2} &= I_{Pm}\cos(\omega t - 60^\circ) + I_{Qm}\cos(\omega t - 150^\circ) \\ &= i_{Ab2} + i_{Rb2}. \end{aligned} \tag{10}$$

Then, active current is composed of i_{Aa2} and i_{Ab2}, which are defined as the first terms of (10), where I_{Pm} is defined as the magnitude of the active current. When the active current transformed into grid side by (5), balanced three-phase current, which is in phase with the grid voltage, is induced. Therefore, the active current can take active power from the grid.

Meanwhile, reactive current is composed of i_{Ra2} and i_{Rb2}, which are defined as the second terms of (10), where I_{Qm} is defined as the magnitude of reactive current. When the reactive current transformed into grid side by (5), three-phase balanced current which is quadrature phase with the grid voltage is induced. Therefore, the reactive current can take reactive power from the grid.

If i_{a2} and i_{b2} are regulated well as described in (4), I_{Pm} and I_{Qm} can be reversely calculated as (11). This calculation is called as active and reactive coordinate transformation (ARCX) in this paper

$$\begin{aligned} I_{Pm} &= i_{a2}\cdot\cos\omega t + \left(\frac{2}{\sqrt{3}}i_{a2} - \frac{1}{\sqrt{3}}i_{b2}\right)\cdot\sin\omega t \\ I_{Qm} &= i_{a2}\cdot\sin\omega t - \left(\frac{2}{\sqrt{3}}i_{a2} - \frac{1}{\sqrt{3}}i_{b2}\right)\cdot\cos\omega t. \end{aligned} \tag{11}$$

By using definition of the currents and ARCX, intuitive relation between grid current and converter-side current can be represented as Fig. 5. The grid current is transformed into d- and q-axis current on the synchronous reference frame as i_{q1}^{e} and i_{d1}^{e} [13]. These currents have a relation with I_{Pm} and I_{Qm} as $i_{q1}^{e} = N_2/N_1 \cdot I_{Pm}$ and $i_{d1}^{e} = N_2/N_1 \cdot I_{Qm}$ as shown in Fig. 5. It matches with the meaning of d, q axes current where each d- and q-axis current controls reactive power and active power, respectively.

For the analysis of power consumption by the active and reactive current, phase diagrams can be depicted as shown in Fig. 6. Line-to-line voltages in grid, e_{ab} and e_{bc}, are transferred to the secondary side of the input transformer as v_a and v_b, as depicted in Fig. 3(a). Phase angles of e_{ab} and e_{bc} are set as 30° and –90° by the phase angles of the grid phase voltages defined above. The phase angles of e_{ab} and e_{bc} are the same with the

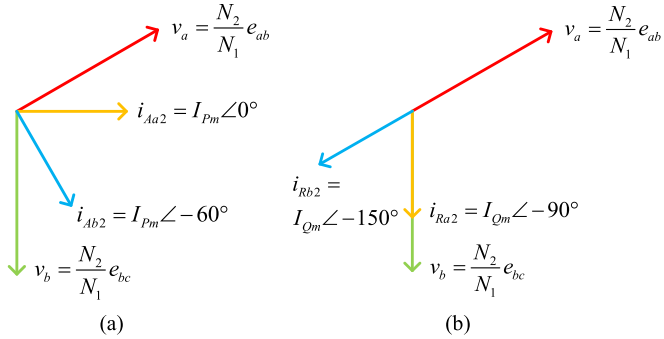

Fig. 6. Phase diagrams of (a) active current and (b) reactive current.

phase angles of v_a and v_b, respectively. The magnitude of grid phase voltage is notated as E_m, then the magnitudes of e_{ab} and e_{bc} are determined as $\sqrt{3}E_m$, and the magnitudes of v_a and v_b are determined as $\sqrt{3}\frac{N_2}{N_1}E_m$. Referring to the phase diagrams, average power consumed by active and reactive current in each cell can be derived as follows:

$$\begin{aligned} P_{Aa} &= \frac{\overrightarrow{v_a}\cdot\overrightarrow{i_{Aa2}}}{2} = \frac{\sqrt{3}}{2}\frac{N_2}{N_1}E_m I_{Pm}\cos(30^\circ) = \frac{3}{4}\frac{N_2}{N_1}E_m I_{Pm} \\ P_{Ab} &= \frac{\overrightarrow{v_b}\cdot\overrightarrow{i_{Ab2}}}{2} = \frac{\sqrt{3}}{2}\frac{N_2}{N_1}E_m I_{Pm}\cos(-30^\circ) = \frac{3}{4}\frac{N_2}{N_1}E_m I_{Pm} \end{aligned} \tag{12}$$

$$\begin{aligned} P_{Ra} &= \frac{\overrightarrow{v_a}\cdot\overrightarrow{i_{Ra2}}}{2} = \frac{\sqrt{3}}{2}\frac{N_2}{N_1}E_m I_{Qm}\cos(120^\circ) \\ &= -\frac{\sqrt{3}}{4}\frac{N_2}{N_1}E_m I_{Qm} \\ P_{Rb} &= \frac{\overrightarrow{v_b}\cdot\overrightarrow{i_{Rb2}}}{2} = \frac{\sqrt{3}}{2}\frac{N_2}{N_1}E_m I_{Qm}\cos(60^\circ) = \frac{\sqrt{3}}{4}\frac{N_2}{N_1}E_m I_{Qm}. \end{aligned} \tag{13}$$

P_{Aa} and P_{Ab}, the average power consumptions of A and B phase cells by the active current, can be derived as (12). Because P_{Aa} and P_{Ab} are the same with each other, the active current can be used to control the average of dc-link voltages of the two cells. Meanwhile, P_{Ra} and P_{Rb}, the average power consumptions of A and B phase cells by the reactive current, are given as (13). Sum of P_{Ra} and P_{Rb} is null, because their magnitudes are the same and their signs are opposite. Therefore, the reactive current can be used to control the difference between the dc-link voltages of the two cells. As the result, by adjusting active current and reactive current, dc-link voltages of a fault operation pair can be controlled independently, while maintaining the grid current to be balanced three-phase sinusoidal current.

B. DC-Link Voltage Controller

Purpose of the dc-link voltage control is to regulate dc-link voltages of a fault operation pair as a reference value under any load conditions. The proposed dc-link voltage controller is composed with two parts: average dc-link voltage controller and dc-link voltage-balancing controller. The average dc-link voltage controller keeps average of the two dc-link voltages as the reference value by regulating the active current. The dc-link

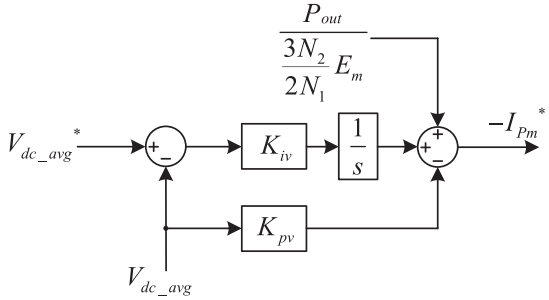

Fig. 7. Average dc-link voltage controller for a fault operation pair.

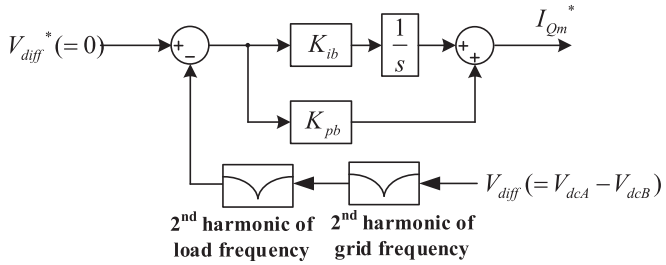

Fig. 8. DC-link voltage-balancing controller for a fault operation pair.

voltage-balancing controller suppresses the difference between the two dc-link voltages by regulating the reactive current.

Average dc-link voltage controller, as shown in Fig. 7, is implemented based on the integral-proportional (IP) controller to prevent overshoot. Its loop equation can be derived as follows:

$$-{I_{Pm}}^* = -K_{pv}V_{\mathrm{dc\_avg}} + K_{iv}\int\left({V_{\mathrm{dc\_avg}}}^* - V_{\mathrm{dc\_avg}}\right)dt + \widehat{P}_{\mathrm{out}}\Big/\frac{3N_2}{2N_1}E_m. \tag{14}$$

For the gain setting of K_{iv} and K_{pv}, control loop analysis for the case of C phase cell fault condition as Fig. 3(a) is considered. The differential term of the energy stored in the dc-link capacitors can be represented as

$$P_{\mathrm{in}} - P_{\mathrm{out}} = \frac{d}{dt}\left(\frac{C_{\mathrm{dc}}}{2}V_{\mathrm{dc}A}^2 + \frac{C_{\mathrm{dc}}}{2}V_{\mathrm{dc}B}^2\right). \tag{15}$$

In this equation, C_{dc} is the dc-link capacitance, and $V_{\mathrm{dc}A}$ and $V_{\mathrm{dc}B}$ are dc-link voltages of A and B phase cells, respectively. P_{in} is the input power from grid and P_{out} is the output power released to the load. The total input power is determined as $P_{\mathrm{in}} = -(P_{Aa} + P_{Ab} + P_{Ra} + P_{Rb}) = -\frac{3N_2}{2N_1}E_m I_{Pm}$. If $V_{\mathrm{dc}A}$ and $V_{\mathrm{dc}B}$ are well regulated according to their reference, ${V_{\mathrm{dc\_avg}}}^*$, the two voltages are almost same and it can be assumed as

$$V_{\mathrm{dc}A}^2 \approx V_{\mathrm{dc}B}^2 \approx V_{\mathrm{dc}A}\cdot V_{\mathrm{dc}B}. \tag{16}$$

Then, (15) can be rewritten as

$$P_{\mathrm{in}} - P_{\mathrm{out}} = \frac{d}{dt}\left(\frac{C_{\mathrm{dc}}}{2}V_{\mathrm{dc}A}^2 + \frac{C_{\mathrm{dc}}}{2}V_{\mathrm{dc}B}^2\right) \approx C_{\mathrm{dc}}\frac{d}{dt}\left(\frac{V_{\mathrm{dc}A}+V_{\mathrm{dc}B}}{2}\right)^2 = C_{\mathrm{dc}}\frac{d{V_{\mathrm{dc\_avg}}}^2}{dt}. \tag{17}$$

If $V_{\mathrm{dc\_avg}}$ is varying near a steady-state value, V_{d0}, then the control loop equation can be derived as (18) under the small-signal analysis

$$C_{\mathrm{dc}}\frac{dV_{\mathrm{dc\_avg}}^2}{dt} = 2C_{\mathrm{dc}}V_{d0}\frac{dV_{\mathrm{dc\_avg}}}{dt} = P_{\mathrm{in}} - P_{\mathrm{out}} = \frac{3N_2}{2N_1}E_m\left(-K_{pv}V_{\mathrm{dc\_avg}} + K_{iv}\int\left({V_{\mathrm{dc\_avg}}}^* - V_{\mathrm{dc\_avg}}\right)dt\right). \tag{18}$$

Then, the transfer function of the controller can be expressed as a form of second-order low-pass filter

$$\frac{V_{\mathrm{dc\_avg}}(s)}{{V_{\mathrm{dc\_avg}}}^*(s)} = \frac{\frac{\frac{3N_2}{4N_1}E_m K_{iv}}{C_{\mathrm{dc}}V_{d0}}}{s^2 + \frac{\frac{3N_2}{4N_1}E_m K_{pv}}{C_{\mathrm{dc}}V_{d0}}s + \frac{\frac{3N_2}{4N_1}E_m K_{iv}}{C_{\mathrm{dc}}V_{d0}}} = \frac{{\omega_n}^2}{s^2 + 2\zeta\omega_n s + {\omega_n}^2}. \tag{19}$$

Finally, IP gain of the controller can be represented with natural frequency and damping factor of the transfer function as

$$K_{pv} = 2\zeta\omega_n\frac{4N_1C_{\mathrm{dc}}V_{d0}}{3N_2E_m}, \quad K_{iv} = {\omega_n}^2\frac{4N_1C_{\mathrm{dc}}V_{d0}}{3N_2E_m}. \tag{20}$$

V_{d0} is recommended to be the reference voltage value, ${V_{\mathrm{dc\_avg}}}^*$. Finally, the control bandwidth would be determined by [13] as

$$\omega_{bw} = \omega_n\cdot\sqrt{(1-2\zeta^2) + \sqrt{4\zeta^4 - 4\zeta^2 + 2}}. \tag{21}$$

DC-link voltage-balancing controller can be implemented based on the PI controller as shown in Fig. 8. As aforementioned, purpose of the controller is to nullify the difference between $V_{\mathrm{dc}A}$ and $V_{\mathrm{dc}B}$, V_{diff}. However, there is an uncontrollable disturbance from fluctuation of each dc-link voltage due to second-order harmonic of the grid frequency and that of load operating frequency. The reason of the fluctuations is the oscillation of power inherent to a single-phase structure of H-bridge used for gird and load connection. For instance, if the grid frequency is 60 Hz and the load frequency is 45 Hz, then there should be 120 and 90 Hz ripples in all dc-link voltages of the single-phase AFE CHB system. The second-order harmonic components are physically impossible to be controlled by any control algorithm; therefore, notch filters for the two frequencies can be installed to block the components in the control loop. On the other hand, the reason why these notch filters are not used in average voltage controller is that the second-order harmonic ripples of $V_{\mathrm{dc}A}$ and $V_{\mathrm{dc}B}$ cancel each other when $V_{\mathrm{dc\_avg}} = (V_{\mathrm{dc}A} + V_{\mathrm{dc}B})/2$ is calculated.

Finally, the dc-link voltage-balancing controller loop equation is expressed as

$${I_{Qm}}^* = K_{pb}({V_{\mathrm{diff}}}^* - V_{\mathrm{diff}}) + K_{ib}\int\left({V_{\mathrm{diff}}}^* - V_{\mathrm{diff}}\right)dt. \tag{22}$$

Difference between energies stored in the dc-link capacitors can be represented as

$$\frac{d}{dt}\left(\frac{C_{\rm dc}}{2}V_{{\rm dc}A}^2-\frac{C_{\rm dc}}{2}V_{{\rm dc}B}^2\right)=P_{{\rm in},A}-P_{{\rm in},B}$$
$$=(-P_{Aa}-P_{Ra})-(-P_{Ab}-P_{Rb})=\frac{\sqrt{3}E_m N_2}{2N_1}I_{Qm}. \quad (23)$$

$P_{{\rm in},A}$ and $P_{{\rm in},B}$ are the cell input power of A and B phase cells, respectively. Assuming that $V_{{\rm dc}A}$ and $V_{{\rm dc}B}$ vary near a steady-state value, V_{d0}, (24) can be derived from (23) by using small-signal analysis

$$\frac{d}{dt}\left(\frac{C_{\rm dc}}{2}V_{{\rm dc}A}^2-\frac{C_{\rm dc}}{2}V_{{\rm dc}B}^2\right)=C_{\rm dc}V_{d0}\frac{d}{dt}(V_{{\rm dc}A}-V_{{\rm dc}B})$$
$$=C_{\rm dc}V_{d0}\frac{d}{dt}V_{\rm diff}. \quad (24)$$

Then, the relation between I_{Qm} and $V_{\rm diff}$ can be extracted from (23) and (24) as

$$I_{Qm}=\frac{2N_1}{\sqrt{3}E_m N_2}C_{\rm dc}V_{d0}\frac{d}{dt}V_{\rm diff}. \quad (25)$$

If I_{Qm} is well regulated as ${I_{Qm}}^*$, (22) and (25) can be combined and (26) can be obtained

$$K_{pb}({V_{\rm diff}}^*-V_{\rm diff})+K_{ib}\frac{{V_{\rm diff}}^*-V_{\rm diff}}{s}$$
$$=\frac{2N_1}{\sqrt{3}E_m N_2}C_{\rm dc}V_{d0}sV_{\rm diff}. \quad (26)$$

Finally, the transfer function and PI gain of balancing controller can be derived as (27) and (28), as a form of second-order low-pass filter

$$\frac{V_{\rm diff}(s)}{{V_{\rm diff}}^*(s)}=\frac{K_{pb}s+K_{ib}}{\frac{2N_1}{\sqrt{3}E_m N_2}C_{\rm dc}V_{d0}s^2+K_{pb}s+K_{ib}}$$
$$=\frac{2\zeta\omega_n s+{\omega_n}^2}{s^2+2\zeta\omega_n s+{\omega_n}^2} \quad (27)$$

where

$$K_{pb}=2\zeta\omega_n\frac{2N_1}{\sqrt{3}E_m N_2}C_{\rm dc}V_{d0},\ K_{ib}={\omega_n}^2\frac{2N_1}{\sqrt{3}E_m N_2}C_{\rm dc}V_{d0}. \quad (28)$$

Also, V_{d0} is recommended to be set the same with ${V_{\rm dc\_avg}}^*$.

C. Current Controller With ARCX

Outputs of the two kinds of dc-link voltage controllers, $-{I_{Pm}}^*$ and ${I_{Qm}}^*$, are used for the inputs of a current controller. Block diagram of a current controller can be represented as shown in Fig. 9, where ω_e is electrical angular speed of grid voltage and L is input inductance.

At the input part of the controller, converter current i_{a2} and i_{b2} are transformed into I_{Pm} and I_{Qm} by the ARCX. PI controllers can be employed for feedback current control, similar with conventional d, q axes PI current controller [14]. The PI gain also can be set in a conventional way. The proportional gain is set as $L\omega_{\rm cc}$ and the integral gain, as $R\omega_{\rm cc}$, where L and R are input inductance and resistance of the system, respectively, and $\omega_{\rm cc}$ is bandwidth of the current controller.

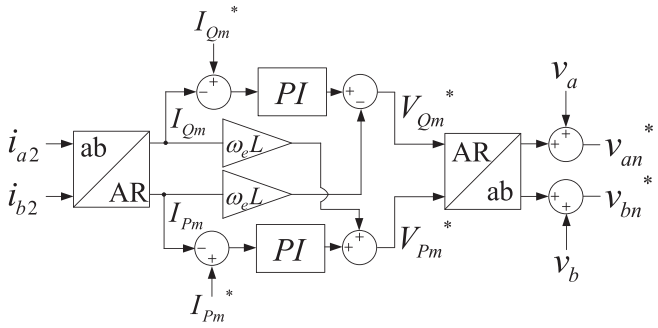

Fig. 9. Block diagram of the current controller for a fault operation pair.

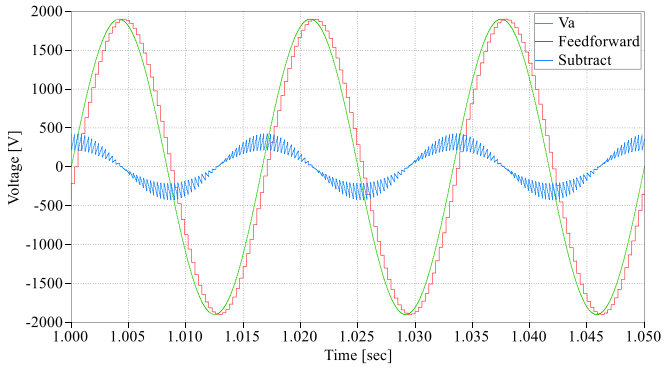

Fig. 10. Subtraction of the grid voltage and its feedforward voltage.

In the conventional controller, a feedforward term for compensating grid voltage is added on q-axis voltage before the inverse coordinate transformation. However, in the proposed current controller, feedforward voltages for compensating the grid voltage should be added after the inverse coordinate transformation. Because the grid voltages transferred to the converter side, v_a and v_b have the same magnitude but 120° phase angle difference, the voltages cannot be expressed in the active and reactive coordinate system. Only the two components that have the same magnitude and 60° phase delay can be expressed in the active and reactive coordinate system.

D. Negative Sequence Current Controller

The grid voltage would be compensated by precalculated feedforwarding term in the current controller. However, due to delay of digital signal processing of the proposed current controller, the grid voltage cannot be perfectly decoupled in the controller as shown in Fig. 10.

In Fig. 10, the sinusoidal green line is one of the transformer secondary-side voltage, v_a, and the red line is its feedforwarding term, $v_{a.\rm ff}$, which is sampled with digital delay. Then, the blue line, $v_{a.\rm err}$, which is subtraction of v_a and its feedforwarding term, appears as grid frequency sinusoidal waveform with the sampling frequency harmonic components. In the case of B phase, v_b, $v_{b.\rm ff}$ and $v_{b.\rm err}$ are lagging as much as 120° compared with v_a, $v_{a.\rm ff}$, and $v_{a.\rm err}$, respectively.

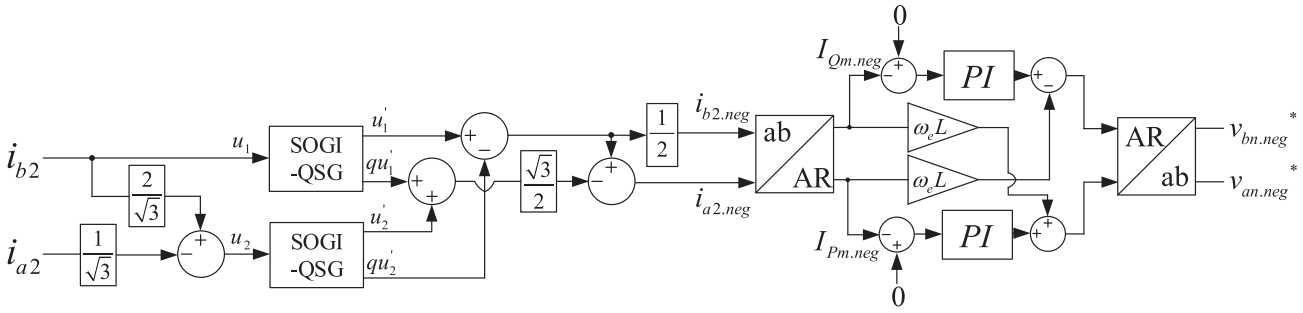

Fig. 11. Block diagram of the negative sequence current controller for a fault operations pair.

In the normal three-phase system, there are three error voltages as $v_{a.\mathrm{err}}, v_{b.\mathrm{err}}$, and $v_{c.\mathrm{err}}$. The voltages would be represented as positive sequence voltage, which makes additional positive sequence current. Therefore, the error voltages can be suppressed by any feedback current controller. However, in the fault operation pair, $v_{a.\mathrm{err}}$ and $v_{b.\mathrm{err}}$ induce the currents, $i_{a2.\mathrm{err}}$ and $i_{b2.\mathrm{err}}$, which have the same magnitude and 120° phase angle difference. $i_{a2.\mathrm{err}}$ and $i_{b2.\mathrm{err}}$ can be divided into two parts as

$$\begin{aligned} i_{a2.\mathrm{err}} &= I_{m.\mathrm{err}}\cos(\omega t+\phi) = \frac{2}{\sqrt{3}} I_{m.\mathrm{err}}\cos(\omega t+\phi-30^\circ) \\ &\quad + \frac{1}{\sqrt{3}} I_{m.\mathrm{err}}\cos(\omega t+\phi+90^\circ) \\ i_{b2.\mathrm{err}} &= I_{m.\mathrm{err}}\cos(\omega t-120^\circ+\phi) \\ &= \frac{2}{\sqrt{3}} I_{m.\mathrm{err}}\cos(\omega t+\phi-90^\circ) \\ &\quad + \frac{1}{\sqrt{3}} I_{m.\mathrm{err}}\cos(\omega t+\phi+150^\circ). \end{aligned} \tag{29}$$

First terms in the right-hand side of $i_{a2.\mathrm{err}}$ and $i_{b2.\mathrm{err}}$ are transformed into positive sequence current in the grid side, but the second terms in right-hand side are negative sequence current by substituting them into (3). Furthermore, unlike the first terms, the second terms cannot be transformed into active and reactive coordinate, so $i_{a2.\mathrm{err}}$ and $i_{b2.\mathrm{err}}$ cannot be removed by the current controller. Therefore, there should be negative sequence current in the grid. Furthermore, i_{a2} and i_{b2} cannot always satisfy (4), because of digital delay or impendence imbalance between phases, etc. Therefore, they could be divided into positive and negative sequence components as follows:

$$\begin{aligned} i_{a2} &= i_{a2.\mathrm{pos}} + i_{a2.\mathrm{neg}} = I_{m.\mathrm{pos}}\cos(\omega t+\phi_p) \\ &\quad + I_{m.\mathrm{neg}}\cos(\omega t+\phi_n-60^\circ) \\ i_{b2} &= i_{b2.\mathrm{pos}} + i_{b2.\mathrm{neg}} = I_{m.\mathrm{pos}}\cos(\omega t+\phi_p-60^\circ) \\ &\quad + I_{m.\mathrm{neg}}\cos(\omega t+\phi_n). \end{aligned} \tag{30}$$

As the result, to make negative sequence current from non-ideal phenomena as null, a negative current controller should be additionally devised as shown in Fig. 11.

Fig. 11 shows the proposed negative sequence current controller. By using dual second-order generalized integrator [15], negative sequence current, $i_{a2.\mathrm{neg}}$ and $i_{b2.neg}$ can be extracted from i_{a2} and i_{b2}. To calculate the values, $I_{Qm.\mathrm{neg}}$ and $I_{Pm.\mathrm{neg}}$, by using ARCX, A and B phase inputs of the transformation are connected to $i_{b2.\mathrm{neg}}$ and $i_{a2.\mathrm{neg}}$, respectively. The output combination is also reversed as ${v_{bn.\mathrm{neg}}}^*$ and ${v_{an.\mathrm{neg}}}^*$ correspond to the A and B phase outputs, respectively. As the result, the input voltage commands for the fault operation pair would be determined as ${v_{an}}^* + {v_{an.\mathrm{neg}}}^*$ and ${v_{bn}}^* + {v_{bn.\mathrm{neg}}}^*$.

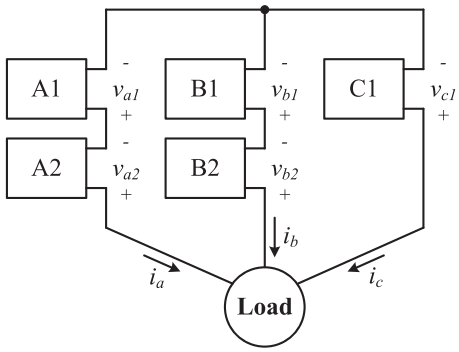

Fig. 12. Output structure of single-phase AFE CHB under 2-2-1 fault condition.

IV. Effect of Load Power Condition on Grid Power Factor

In the general back-to-back systems, although there is negative sequence current, harmonic current or reactive power in the load side, it would be filtered out by the dc-link capacitor. Thus, the harmonics and the power factor of the load could not be reflected to grid side. However, in the case of using the proposed fault operation of the single-phase AFE CHB system, the power factor of the load would affect the grid power factor. To analyze the phenomenon, the system output structure under 2-2-1 fault condition is assumed as shown in Fig. 12. It is assumed that the output voltage of the CHB is modulated according to the control schemes proposed in [7] under cell fault condition. The phase diagram considering power factor angle of the load can be depicted as Fig. 13.

As shown in Fig. 13, line-to-line voltage of three-phase maintains balanced under the cell fault condition. Red-colored vectors correspond to the output voltages of A1, B1, and C1 cells, v_{a1}, v_{b1}, and v_{c1}. They have the same magnitude and 120° angle shift to each other. If the load current, i_a, i_b, and i_c, is balanced,

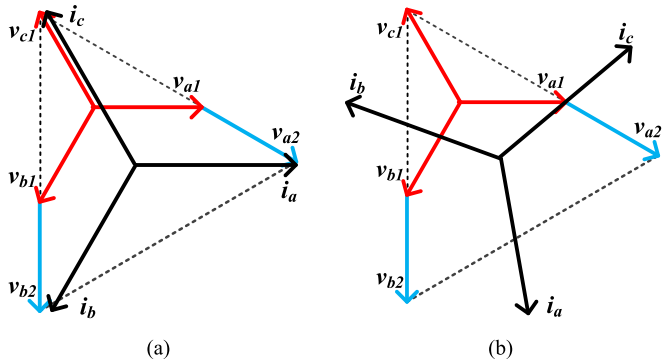

Fig. 13. Phase diagrams under the 2-2-1 fault condition by load power factor angle. (a) 0°. (b) 80° lagging.

regardless of the load power factor, each cell always has the same power factor and it can be expressed with load power factor angle θ_L as

$$\begin{aligned}\cos(\theta_{va1} - \theta_{ia}) &= \cos(\theta_{vb1} - \theta_{ib}) \\ &= \cos(\theta_{vc1} - \theta_{ic}) = \cos(\theta_L). \end{aligned} \tag{31}$$

In (31), $\theta_{va1}, \theta_{vb1}$, and θ_{vc1} are the phase angles of v_{a1}, v_{b1}, and v_{c1}, respectively. θ_{ia}, θ_{ib}, and θ_{ic} are the phase angles of i_a, i_b, and i_c, respectively.

On the other hand, cells in fault operation pair, A2 and B2, make phase voltages which correspond to the blue-colored vectors, v_{a2} and v_{b2}, as the same magnitude and 60° delay. Therefore, their power factors are different according to load power factor angle as

$$\begin{aligned} pf_{A2} &= \cos(\theta_{va2} - \theta_{ia}) = \cos(\theta_L - 30^\circ) \\ pf_{B2} &= \cos(\theta_{vb2} - \theta_{ib}) = \cos(\theta_L + 30^\circ). \end{aligned} \tag{32}$$

In (32), θ_{va2} and θ_{vb2} are the phase angles of v_{a2} and v_{b2}, respectively. pf_{A2} and pf_{B2} are output power factors of A2 and B2 cells, respectively. When the load power factor angle, θ_L, is 0° or 180°, then pf_{A2} and pf_{B2} are the same. However, in other cases, they do not match to each other. Even the $\cos(\theta_L)$ becomes zero, the difference between pf_{A2} and pf_{B2} gets the maximum. For instance, in the case of $\theta_L = 80°$ lagging, as shown in Fig. 13(b), $pf_{A2} = 0.643$ and $pf_{B2} = -0.342$ which means that A2 cell is supplying power to the load, but B2 cell is getting power from the load. Under this condition, large reactive current for the balancing of dc-link voltages of the two cells is required and it would be transformed into d-axis current of the grid. Therefore, in the fault operation, the load power factor has an influence on the grid power factor. However, in most cases, the load power factor would be close to 1, so it could not be a severe problem. Furthermore, if there is current margin in the normal operation pairs, the d-axis current in the grid, come from the fault operation pair, could be compensated by the normal operation pairs. As the result, the grid power factor also can be regulated as one in spite of the proposed operation of the fault operation pairs.

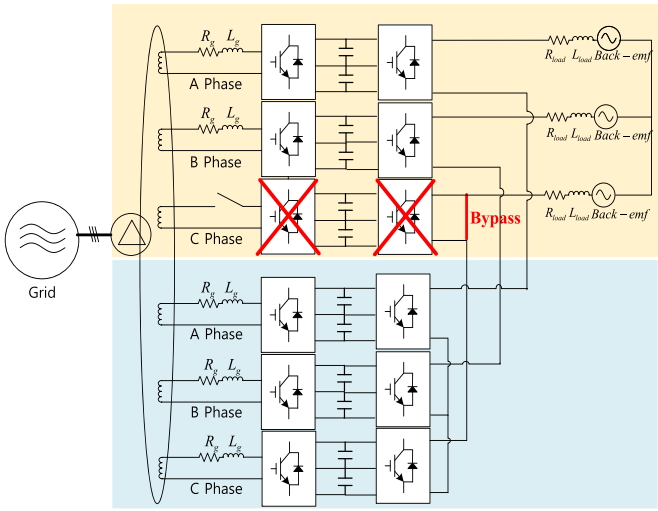

Fig. 14. Full structure of single-phase AFE CHB system under 2-2-1 fault condition.

TABLE I
GRID PARAMETERS

Capacity	*Line-to-line Voltage*	*Frequency*
1.066MVA	22900 V_{rms}	60 Hz
Transformer Turn Ratio	***Input Resistance***	***Input Inductance***
18.75 : 1	83.9 mΩ (0.01p.u.)	1.3 mH (0.06p.u.)

TABLE II
INDUCTION MOTOR RATED CONDITION

Capacity	*Line-to-line Voltage*	*Frequency*	*Pole number*	*Motor type*
0.833 MW	4400 V_{rms}	60 Hz	8 pole	B type [13]

V. SIMULATION AND EXPERIMENTAL RESULTS

A. Simulation Results

As shown in Fig. 14, the simulation model is designed as 2-2-1 fault condition. It is assumed that upper C phase cell is excluded from the system due to cell fault and its output terminal is bypassed. The input power control is implemented with the division of the input structure into a fault operation pair and a normal operation pair. The simulation set has a difference compared with Fig. 1 that there are two series-connected capacitors at the dc link of each cell. The reason is that the legs that constitute the power cells are three-level neutral-point clamped (NPC) legs to reduce the number of cells in each phase. Finally, the load implies an induction motor drive system with variable voltage variable frequency control. The system parameters of the grid and the load are provided in Table I and Table II, respectively.

Following load operation scheme in [7], maximum line-to-line voltage is 78.8% of rated line-to-line voltage under

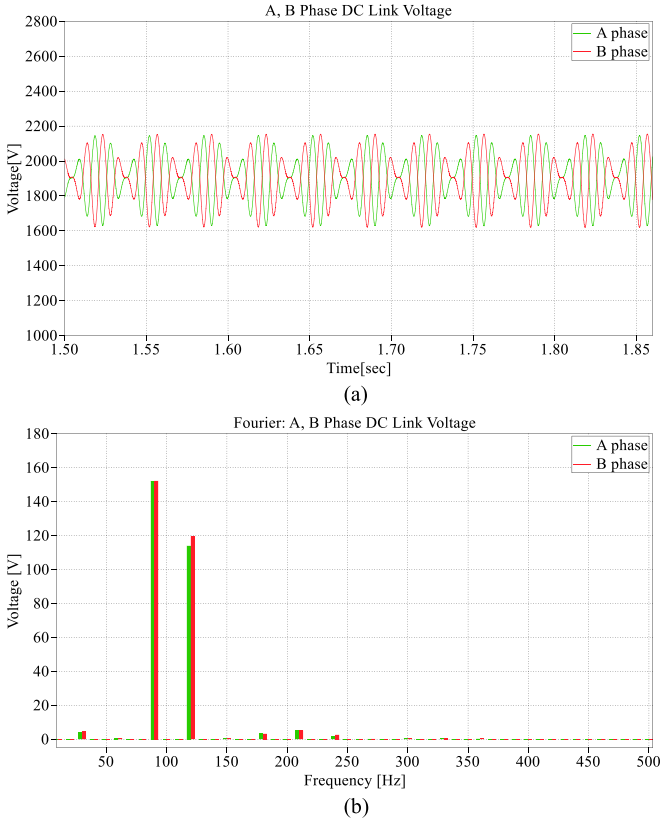

Fig. 15. (a) DC-link voltages of the fault operation pair and (b) its Fourier spectrum.

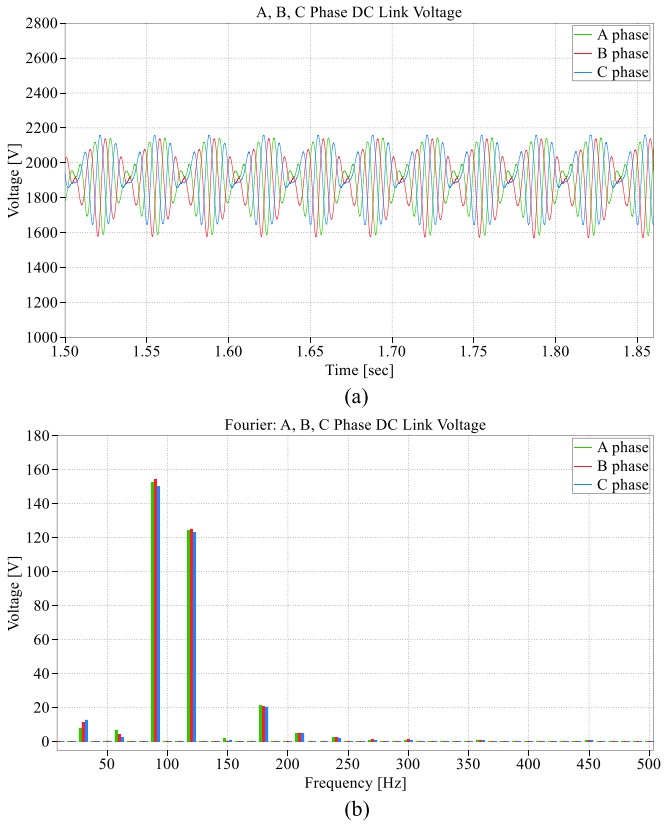

Fig. 16. (a) DC-link voltages of the normal operation pair and (b) its Fourier spectrum.

2-2-1 fault condition. Therefore, the induction motor is driven at 75% of rated speed, 45 Hz. Switching frequency of each leg is 1620 Hz. DC-link capacitance in a cell is 900 μF in total, and the reference of dc-link voltage is set to 1900 V.

In Figs. 15 and 16, it is shown that the average dc-link voltages of the fault operation pair and the normal operation pair both are correctly kept as 1900 V. The ripples in the two kinds of dc-link voltages are mainly composed of 90 and 120-Hz frequency components which are two times of load frequency (f_{load}) and grid frequency (f_{grid}), respectively. As aforementioned, it is quite difficult to suppress these ripples by a voltage controller. Also, there are some other ripples as shown in Figs. 15(b) and 16(b), which can be represented as (33), where f_{dc} is any possible ripple frequency of dc-link voltage

$$f_{\text{dc}} = 2 \cdot k \cdot f_{\text{grid}} + 2 \cdot q \cdot f_{\text{load}} \ (\text{where} \ \ k, q \ \ \text{are integer}). \tag{33}$$

The line-to-line voltage to the motor is shown in Fig. 17. Each voltage has 17 levels for AB phase, 13 levels for BC and CA phase because of a faulty cell in C phase. It is confirmed that the fundamental frequency of the voltages is well balanced and the equivalent magnitude is 3292 V_{rms}, almost 75% of rated voltage as expected.

As shown in Fig. 18(a), the input ac of the fault operation pair is well controlled with the proposed method, as the two phase input currents of the fault operation pair have the same magnitudes and 60° phase delay. In Fig. 18(b), the three-phase input

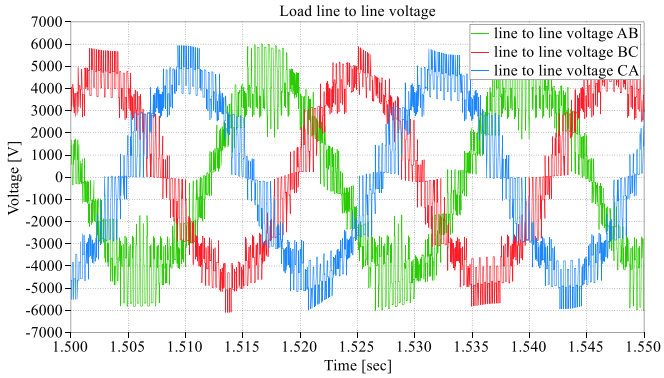

Fig. 17. Output line-to-line voltages of the inverter.

currents of the normal operation pair are also well controlled with the same magnitudes and 120° phase delay.

To verify the circulating current calculated by (9), simulations have been carried out as Fig. 19. By (2), i_{circ} can be calculated as the average of the primary delta winding current. The magnitude of input currents, i_{a2} and i_{b2} in Fig. 18(a), is 171.6 A. The turn ratio of the input transformers, N_1/N_2 is 22 900/1221. Then, the magnitude of the induced circulating currents $|i_{\text{circ}}|$ is calculated as 5.28 A. The magnitude of the circulating current measured in the simulation result is about 5.29 A. It is well matched to the calculated value.

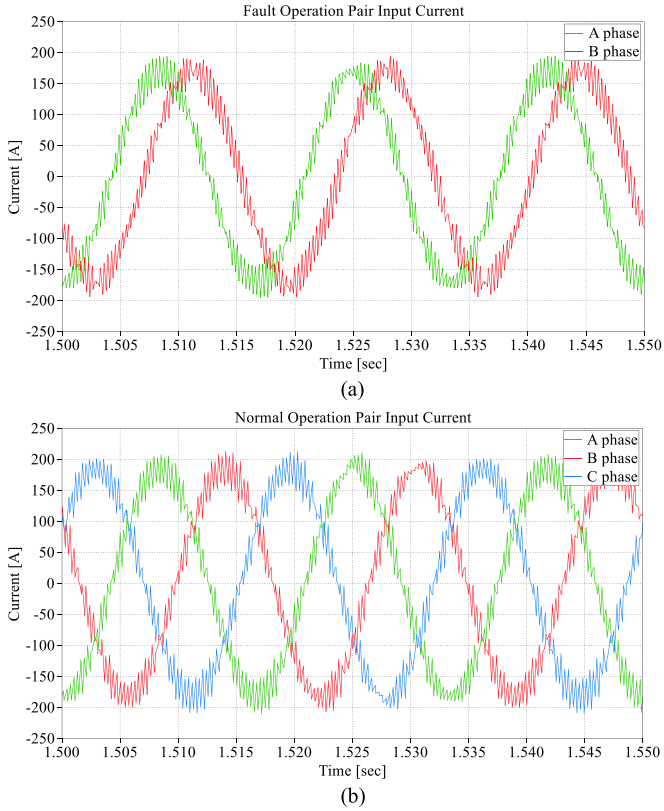

Fig. 18. Input current of (a) fault operation pair and (b) normal operation pair.

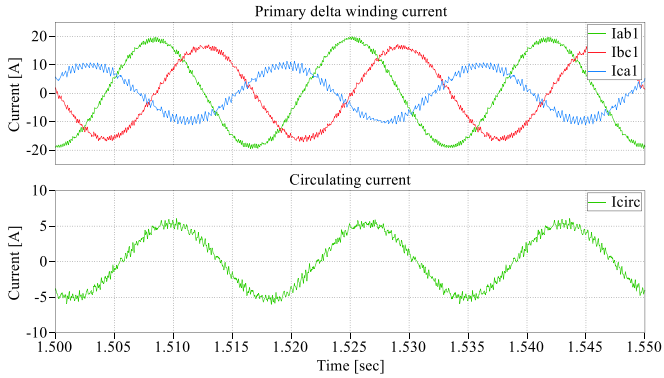

Fig. 19. Primary delta winding current and the circulating current.

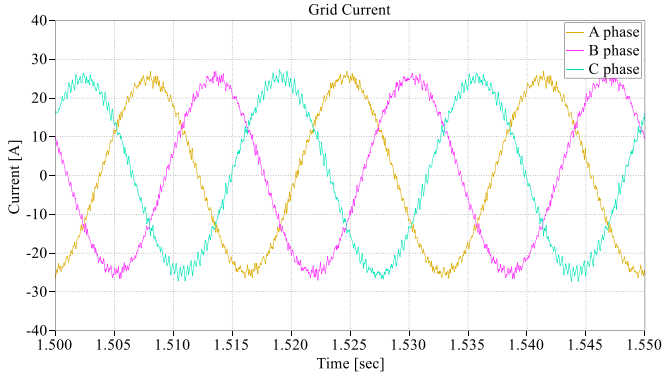

Fig. 20. Three-phase grid current.

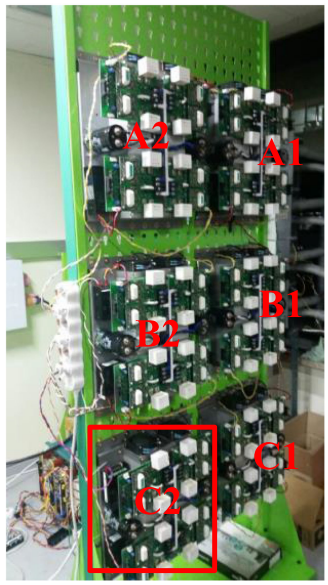

Fig. 21. Single-phase AFE CHB experimental set for induction machine drive.

TABLE III
SYSTEM PARAMETERS

Number of Cell	6
Source Voltage	127 V_{rms}
Cell input voltage	110 V_{rms}
DC link Capacitance	1650 μF
Rated Output Voltage	440 V_{rms}
Rated frequency	60 Hz
Switching frequency for one leg	2.5 kHz
Rated Cell power	2.7 kVA

In Fig. 20, it is clearly shown that the grid current is well regulated as three-phase balanced sinusoidal waveform even under the cell fault condition.

B. Experimental Results

Experimental set shown in Fig. 21 has the same structure with that of simulation as 2-2-1 fault condition and three-level NPC legs with two series dc-link capacitors. The system parameters of the experimental set are provided in Table III. C2 cell in the red box is assumed as a faulty cell, and its input terminal is disconnected from the grid and its output terminal is bypassed. With remaining cells, A1, B1, and C1 cells are driven with the normal operation method [10], and A2 and B2 cells are driven with the proposed fault operation method. Source voltage 127 V_{rms} is changed into 110 V_{rms} by an input transformer and there is no additional filter to reduce harmonics of grid current. Three-phase output of the system is connected to 440 V_{rms}, 11 kW, four-pole induction motor. Load torque to the induction motor is applied by a 20-kW dc generator.

Fig. 22 shows the dc-link voltages and input ac of the fault operation pair in the start-up situation. When the system is in

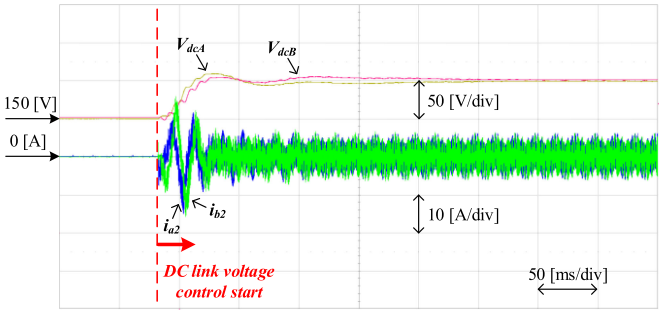

Fig. 22. DC-link voltages and input current of the fault operation pair in the start-up situation.

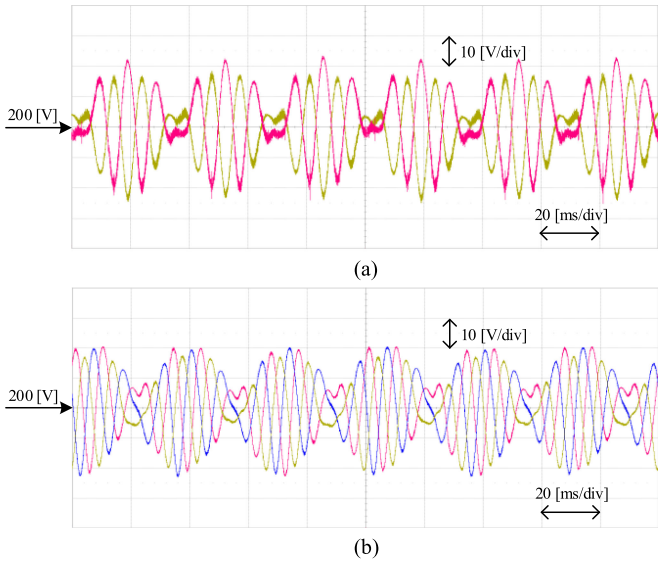

Fig. 23. DC-link voltages of (a) fault operation pair and (b) normal operation pair.

OFF state, the dc-link voltages, $V_{\mathrm{dc}A}$ and $V_{\mathrm{dc}B}$, are charged by the freewheeling diodes as much as 155 V, because the single-phase input voltage is 110 $\mathrm{V_{rms}}$. After engaging the proposed control algorithm with the dc-link voltage controller, the dc-link voltages are regulated as 200 V. While both dc-link voltages increase, ac i_{a2} and i_{b2} increase. In this boosting operation, the maximum value of the currents in the transient is about 15 A and phase difference between i_{a2} and i_{b2} is well controlled as 60°. After boosting the dc-link voltage, the dc-link voltages are kept as their reference, 200 V, and the reference of the ac is nearly nullified.

In the steady states, dc-link voltage of each cell is controlled as 200 V, and dc-link voltages of a fault operation pair and a normal operation pair are shown in Fig. 23. As expected, there are some oscillations in the second-order harmonics of 60 and 45 Hz, which are grid and load frequency, respectively.

Induction motor is driven at 45 Hz, so the input line-to-line voltage is modulated as three-fourth of rated voltage as 330 $\mathrm{V_{rms}}$ $(= 466\ \mathrm{V_{pk}})$. The output phase voltage is modulated according to the scheme in [7], and the voltage is depicted in Fig. 24(a). v_{cn} has five levels because only one cell is left in C phase. As described in Fig. 24(b), the fundamental frequency

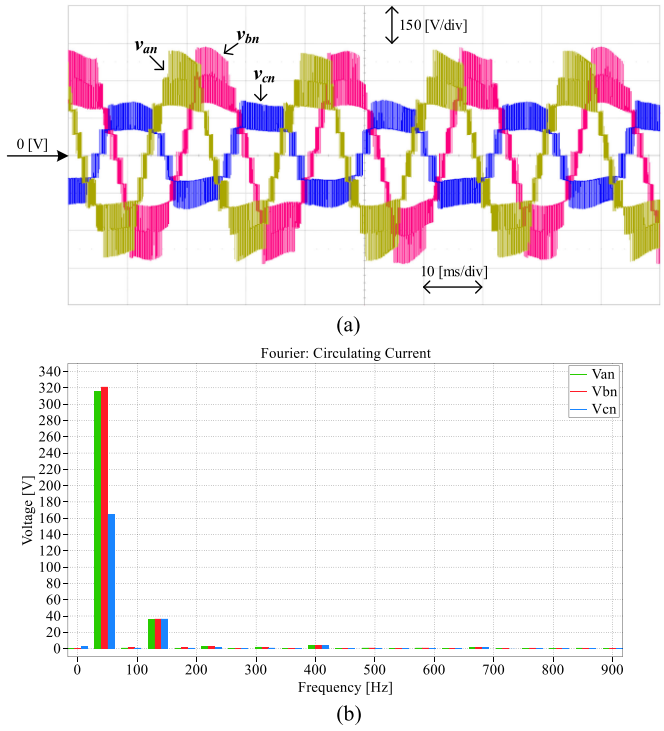

Fig. 24. (a) Output phase voltage of the CHB system and (b) its Fourier spectrum.

amplitude of v_{an}, v_{bn}, and v_{cn} are 315.1, 321.1, and 164.2 V, respectively, that the load control scheme in [7] is implemented well. There is some third harmonic component in the phase voltage made by the offset voltage, which would not be in line-to-line voltage at the load.

As the result, output line-to-line voltage is modulated as Fig. 25(a). By the Fourier transform, v_{ab}, v_{bc}, v_{ca} peak values are measured as almost the same as 451, 454, and 449 V and the phase differences are 120°. From Fig. 25(b), it can be said that the three-phase balanced line-to-line voltage is applied to the load. Also, the large number of the voltage levels makes the harmonic components be small. On the other hand, the load torque from dc generator is set as 90% of the rated value, so the power supplied from the converter is about 68% of rated power of the motor, which is about 7.5 kW.

With the proposed current control strategy, not only input current of the normal operation pair but also that of the fault operation pair are well controlled as shown in Fig. 26.

To verify the circulating current by (9), experimental test also has been carried out and the result is shown in Fig. 27. By (2), i_{circ} can be calculated as the average of the primary delta winding current. The magnitude of input currents, i_{a2} and i_{b2} in Fig. 26(a), is 26.5 A. The turn ratio of the input transformers, N_1/N_2, is 127/110. Then, the magnitude of the induced circulating currents, $|i_{\mathrm{circ}}|$, is calculated as 13.3 A by (9) while the magnitude of the circulating current in the experimental test is about 10.7 A as shown in Fig. 27(b). The simulation result exactly matches with the theoretical value, but the experimental result is smaller than the theoretical value. The reason would be the nonideal characteristic of the transformer such as magnetizing

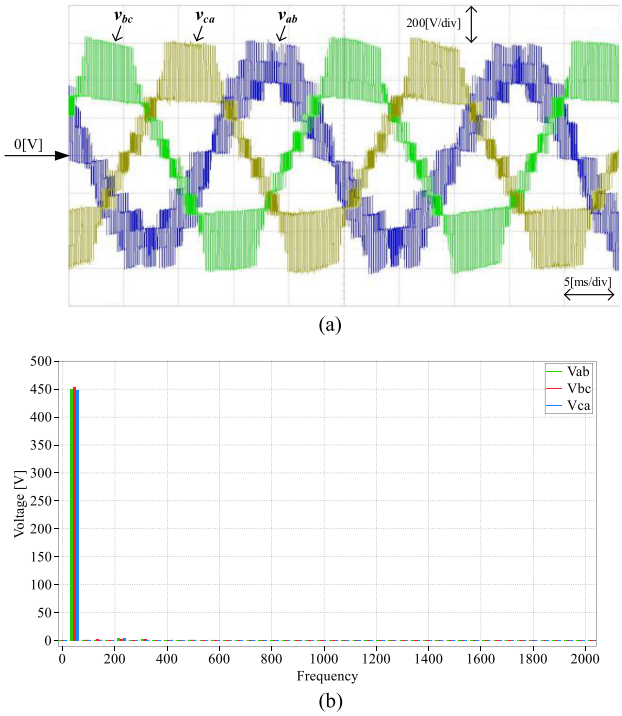

Fig. 25. (a) Output line-to-line voltage of the CHB and (b) its Fourier spectrum.

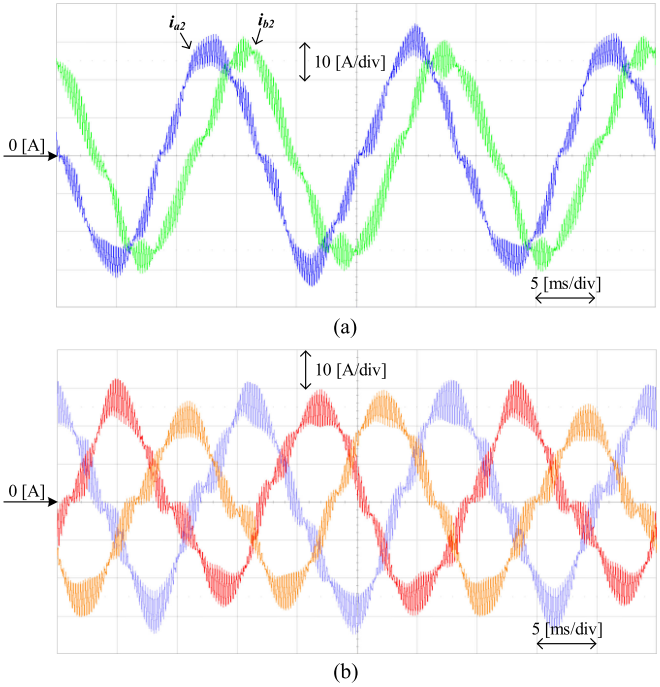

Fig. 26. Input current of (a) fault operation pair and (b) normal operation pair.

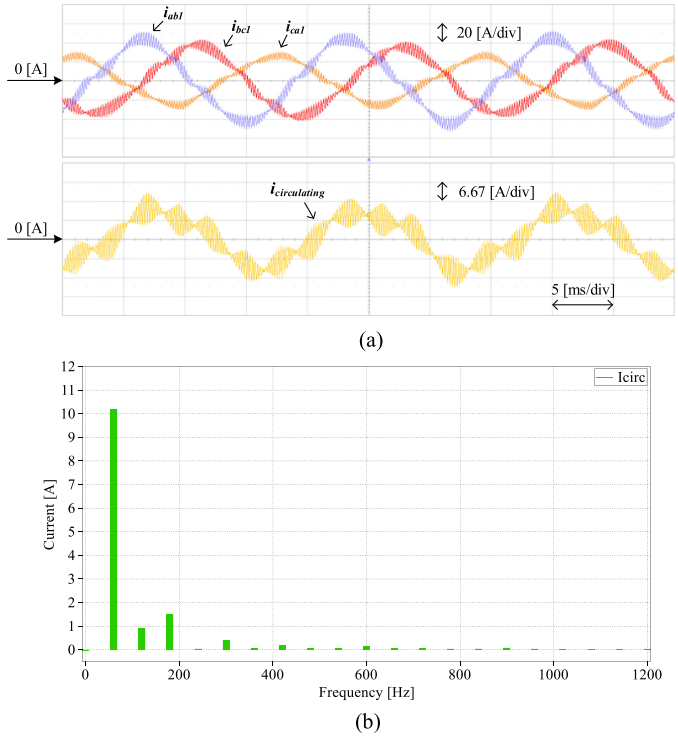

Fig. 27. (a) Primary delta winding current, the circulating current, and (b) Fourier spectrum of the circulating current.

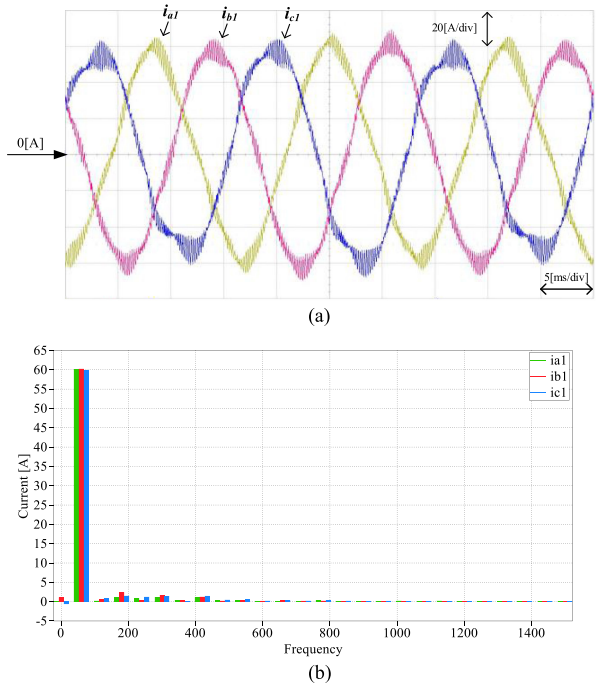

Fig. 28. (a) Three-phase balanced grid current and (b) its Fourier spectrum.

inductance, saturation effect, leakage fluxes, and unbalance of each phase. On the other hand, there is some third harmonic components in the circulating current, which would come from the excitation current of the transformer.

Finally, it is demonstrated that three-phase balanced current flows in the grid as shown in Fig. 28(a) even under the cell fault condition. By the Fourier spectrum of the grid current, Fig. 28(b), there are some low-order harmonic components because of the impedance unbalance and magnetic saturation of the input multiwinding transformer. The harmonics are less than 4% of the rated current of the CHB converter, and those are under the limit of most harmonic standards such as IEEE 519.

VI. Conclusion

This paper analyzes the relation between the grid current and converter current of the single-phase AFE CHB, and figures out what converter current should flow under the cell fault condition to make the grid current be balanced. Based on the analysis, a novel scheme for reconfiguration of healthy cells has been proposed. By the virtue of the reconfiguration, the power capacity of AFE CHB can be maximally exploited without turning OFF the healthy cells to make the number of operating cells in each phase the same. Accepting different number of cells in each phase, the dc-link voltage controller of a fault operation pair has been newly devised. Furthermore, positive and negative current control schemes for the fault operation pair have been also proposed to make the grid current be balanced and harmonic free. All control schemes have been verified through full-scale computer simulation and reduced size experimental tests. The result reveals well-controlled dc-link voltage of a fault operation pair and sinusoidal balanced grid current under the cell fault condition. Thanks to the proposed reconfiguration and control, the output power of the CHB under 2-2-1 cell fault condition has been extended utmost from 50% to 78.8% of the rated power.

References

[1] P. Hammond, "A new approach to enhance power quality for medium voltage AC drives," *IEEE Trans. Ind. Appl.*, vol. 33, no. 1, pp. 202–208, Jan./Feb. 1997.

[2] M. Malinowski, K. Gopakumar, J. Rodriguez, and M. Perez, "A survey on cascaded multilevel inverters," *IEEE Trans. Ind. Electron.*, vol. 57, no. 7, pp. 2197–2206, Jul. 2010.

[3] H. S. Jung, J. M. Yoo, S. K. Sul, H. J. Lee, and C. Hong, "Parallel operation of inverters with isolated DC link for minimizing sharing inductor," *IEEE Trans. Ind. Appl.*, vol. 53, no. 5, pp. 4450–4459, Sep./Oct. 2017.

[4] H. S. Jung, J. M. Yoo, S. K. Sul, H. J. Lee, and C. Hong, "Suppression of circulating current in paralleled inverters with isolated DC-link," in *Proc. IEEE Energy Convers. Congr. Expo.*, Milwaukee, WI, USA, 2016, pp. 1–8.

[5] P. Lezana and G. Oritz, "Extended operation of cascade multicell converters under fault condition," *IEEE Trans. Ind. Electron.*, vol. 56, no. 7, pp. 2697–2703, Jul. 2009.

[6] P. Hammond, "Multiphase power supply with series connected power cells with failed cell bypass," US Patent 6 222 284 B1, Apr. 24, 2001.

[7] P. Correa, M. Pacas, and J. Rodriguez, "Modulation strategies for fault-tolerant operation of H-bridge multilevel inverters," in *Proc. IEEE Int. Symp. Ind. Electron.*, vol. 2, Jul. 2006, pp. 1589–1594.

[8] P. Lezana, R. Rodriguez, and D. A. Oyarzun, "Cascaded multilevel inverter with regeneration capability and reduced number of switches," *IEEE Trans. Ind. Electron.*, vol. 66, no. 3, pp. 1059–1066, Mar. 2008.

[9] T. Oka, H. Kusunoki, M. Tsukakoshi, J. Kleinecke, and M. Daskalos, "Active front-end topology for 5 level medium voltage drive system with isolated DC bus," in *Proc. Int. Power Electron. Conf.*, May 2014, pp. 2330–2335.

[10] J.-M. Yoo, H.-S. Jung, and S.-K. Sul, "DC link voltage control of single phase back-to-back converter for medium voltage motor drive," in *Proc. Int. Power Electron. Motion Control Conf.*, May 2016, pp. 3043–3049.

[11] B. Bahrani, A. Rufer, S. Kenzelmann, and L. Lopes, "Vector control of single-phase voltage-source converters based on fictive-axis emulation," *IEEE Trans. Ind. Appl.*, vol. 47, no. 2, pp. 831–840, Mar./Apr. 2011.

[12] O. Alavi, A. H. Viki, and S. Shamlou, "A comparative reliability study of three fundamental multilevel inverters using two different approaches," *Electronics*, vol. 5, no. 2, pp. 1–18, 2016.

[13] S.-K. Sul, *Control of Electric Machine Drive Systems*, 2nd ed. New York, NY, USA: Wiley, 2011, ch. 3.

[14] M. Liserre, R. Teodorescu, and F. Blaabjerg, "Multiple harmonics control for three-phase grid converter systems with the use of PI-RES current controller in a rotating frame," *IEEE Tran. Power Electron.*, vol. 21, no. 3, pp. 836–841, May 2006.

[15] P. Rodriguez, "New positive-sequence voltage detector for grid synchronization of power converters under faulty grid conditions," in *Proc. IEEE Power Electron. Spec. Conf.*, Jun. 2006, pp. 1–7.

[16] Y.-R. Lee, J.-M. Yoo, H.-S. Jung, and S.-K. Sul, "Control strategy of single phase back-to-back converter for MV drive under the cell fault condition," in *Proc. Energy Convers. Congr. Expo.*, Sep. 2016, pp. 1–6.

Yoon-Ro Lee (S'16) was born in Anyang, South Korea, in 1992. He received the B.S. and M.S. degrees in electrical engineering and computer science from Seoul National University, Seoul, South Korea, in 2015 and 2017, respectively, where he is currently working toward the Ph.D. degree in electrical engineering.

His current research interests include power electronics for control of electrical machines, emulation of electrical machines, design and control of power conversion systems.

Jeong-Mock Yoo (S'14–M'16) was born in South Korea in 1991. He received the B.S. and M.S. degrees in electrical engineering from Seoul National University, Seoul, South Korea, in 2014 and 2016, respectively.

He is currently a Research Engineer with LG Electronics, Seoul. His research interests include electric machine drive systems and design and control of power converters for automotive application.

Hyun-Sam Jung (S'11) received the B.S. and M.S. degrees in electrical engineering and computer science from Seoul National University, Seoul, South Korea, in 2010 and 2012, respectively, where he is currently working toward the Ph.D. degree in electrical engineering.

In 2012, he joined Samsung Heavy Industries Company, Ltd., South Korea, where he worked three years. His current research interests include power electronics control of electrical machines and power-converter circuits.

Seung-Ki Sul (S'78–M'87–SM'98–F'00) received the B.S., M.S., and Ph.D. degrees in electrical engineering from Seoul National University, Seoul, South Korea, in 1980, 1983, and 1986, respectively.

From 1986 to 1988, he was an Associate Researcher with the Department of Electrical and Computer Engineering, University of Wisconsin, Madison. From 1988 to 1990, he was a Principal Research Engineer with LG Industrial Systems Company, South Korea. Since 1991, he has been a Member of Faculty of the School of the Electrical and Computer Engineering, Seoul National University, where he is currently a Professor. He has authored or coauthored more than 150 IEEE journal papers and a total of more than 340 international conference papers in the area of power electronics. He holds 14 US patents, 7 Japanese patents, 11 Korean patents, and granted 43 Ph.D.s under his supervision. His current research interests include power electronic control of electrical machines, electric/hybrid vehicles and ship drives, high-voltage dc transmission based on the modular multilevel converter, and power-converter circuits for renewal energy sources.

Dr. Sul was the Program Chair of IEEE Power Electronics Specialists Conference 2006 and the General Chair of IEEE Energy Conversion Congress and Exposition-Asia, International Conference on Power Electronics, 2011. In 2015, he was the President of the Korean Institute of Power Electronics. He was the recipient of 2015 IEEE Transaction 1st and 2nd Paper Awards on Industrial Application, simultaneously. He was also recipient of 2016 Outstanding Achievement Award of IEEE Industrial Application Society and the recipient of 2017 Newell Award of IEEE Power Electronics Society.